Atmospheric wind and temperature profiles inversion using infrasound: an ensemble model context

Ismael Vera Rodriguez[1,1], Sven Peter Näsholm[2,2], and Alexis Le Pichon[3,3]

[1]NORSAR
[2]Norsar
[3]CEA, DAM, DIF

November 30, 2022

Abstract

We present an inversion methodology aimed at updating an atmospheric model to be consistent with a set of infrasound-derived observations. Compared to previous approaches, we sought to apply a more flexible parameterization. This permits to incorporate physical and numerical constraints without the need to reformulate the inversion. On the other hand, the optimization conveys an explicit search over the solution space, making the solver computationally expensive. Nevertheless, through a parallel implementation and the use of tight constraints we demonstrate that the methodology is computationally tractable. Constraints to the solution space are derived from the spread (variance) of ERA5 ensemble reanalysis members, which summarize the best current knowledge of the atmosphere from assimilated measurements and physical models. Similarly, the initial model temperature and winds for the inversion are chosen to be the average of these parameters in the ensemble members. The performance of the inversion is demonstrated with the application to infrasound observations from an explosion generated by the destruction of ammunition at Hukkakero, Finland. The acoustic signals are recorded at an array station located at 178 km range, which is within the classical shadow zone distance. The observed returns are assumed to come from stratospheric reflections. Therefore, in this example, the altitude of reflection is also an unknown that is inverted for, together with the updated atmospheric model.

Atmospheric wind and temperature profiles inversion using infrasound: an ensemble model context

I. Vera Rodriguez [1] *, S. P. Näsholm [1] and A. Le Pichon [2]

[1] *NORSAR, Department of Applied Seismology, Kjeller, Norway*

[2] *CEA, DAM, DIF, Arpajon, France*

SUMMARY

We present an inversion methodology aimed at updating an atmospheric model to be consistent with a set of infrasound-derived observations. Compared to previous approaches, we sought to apply a more flexible parameterization. This permits to incorporate physical and numerical constraints without the need to reformulate the inversion. On the other hand, the optimization conveys an explicit search over the solution space, making the solver computationally expensive. Nevertheless, through a parallel implementation and the use of tight constraints we demonstrate that the methodology is computationally tractable. Constraints to the solution space are derived from the spread (variance) of ERA5 ensemble reanalysis members, which summarize the best current knowledge of the atmosphere from assimilated measurements and physical models. Similarly, the initial model temperature and winds for the inversion are chosen to be the average of these parameters in the ensemble members. The performance of the inversion is demonstrated with the application to infrasound observations from an explosion generated by the destruction of ammunition at Hukkakero, Finland. The acoustic signals are recorded at an array station located at 178 km range, which is within the classical shadow zone distance. The ob-

served returns are assumed to come from stratospheric reflections. Therefore, in this example, the altitude of reflection is also an unknown that is inverted for, together with the updated atmospheric model.

Key words: Infrasound – classical shadow zone – ensemble reanalysis model – model inversion

1   INTRODUCTION

This work considers the problem of estimating an updated atmospheric model to become consistent with a set of infrasound observations, and the associated problem of identifying the member(s) from an atmospheric reanalysis model ensemble that lie closer to the infrasound-consistent, updated model.

Atmospheric reanalysis models are the result of the assimilation of direct and indirect measurements of different properties of the atmosphere (e.g., Uppala et al. 2005; Kazutoshi et al. 2007; Parker 2016). For example, direct measurements of atmospheric winds and temperature are provided by radiosondes up to altitudes of around 30 km. Satellites, on the other hand, provide measurements from which estimations of temperature can be obtained up to altitudes of ~50 km (Lee et al. 2019).

A better representation of the upper stratosphere in models, especially for winds, can contribute to an enhanced numerical weather prediction on weekly to monthly timescales, especially during winter (see e.g., Domeisen et al. 2020a,b, and the references therein). To this end, efforts are made to adapt and expand atmospheric probing infrastructures and technologies to provide additional measurements on the dynamics of the stratosphere (e.g., Tan et al. 2008; Blanc et al. 2018, 2019; Khaykin et al. 2020).

Over the last decade, there have been significant improvements in global data assimilation capabilities of the lower, middle, and upper atmosphere (Drob 2019). General circulation models (GCMs) have been progressively extended to cover the whole stratosphere to better capture stratospheric-tropospheric interactions and improve forecast skill scores (Charlton-Perez et al. 2013; Siskind & Drob 2014). However, the mean state and the variability described by Numerical Weather Prediction (NWP) models, such as those distributed by the European Centre for Medium-Range Weather Forecasts (ECMWF), are subject to inaccuracies in both cur-

⋆ NORSAR, Norway

rent operational analyses and reanalyses in the altitude range where assimilated observations become sparser (i.e., above 30 km altitude).

Within the Copernicus Climate Change Service (C3S), ECMWF is producing the ERA5 reanalysis, which embodies a detailed record of the global atmosphere. This new reanalysis, based on the Integrated Forecasting System (IFS) Cy41r2, benefits from a decade of developments in model physics, core dynamics and data assimilation. A gain in forecast skills has been shown (Hersbach et al. 2020), allowing an enhanced description of the evolution of weather systems in the troposphere. ERA5 also provides analyses with better global-mean temperatures in the uppermost troposphere and stratosphere, although it still suffers from temperature uncertainty and bias (Simmons et al. 2020).

There is a current interest from the NWP community to validate model specifications at stratospheric altitudes using independent observations. This includes satellite radiance and additional high-resolution measurements (gravity waves and momentum flux) that are currently not resolved in gravity wave model parameterization schemes (e.g., Charlton-Perez et al. 2013). Given the importance of model validation in the middle and upper atmosphere regions, recent studies focused on comparisons between ECMWF products with independent observations such as long-duration balloon flights (e.g., Podglajen et al. 2014). Wind radiometer and lidar instruments were also used to evaluate the accuracy of NWP models and data-constrained assimilation systems (e.g., Le Pichon et al. 2015; Ehard et al. 2017). The development of innovative high-resolution prototype sounding systems providing in near-real time wind and temperature observations from the ground to the mesosphere and lower-thermosphere (MLT) has stimulated the construction of multi-technology observational platforms detailing the dynamics of the middle atmosphere and interactions between atmospheric layers with unprecedented resolution (Blanc et al. 2018).

Infrasound waves provide complementary information to characterize the middle atmosphere. This is particularly valuable above 30 km altitude where few other currently available technologies provide direct measurements, especially for the dynamics (see e.g., Le Pichon et al. 2019, for a review). As infrasonic waves propagate into the middle atmosphere, small-scale features of the vertical structure of the atmosphere can also be inferred from the characteristics of measured wave parameters (Chunchuzov & Kulichkov 2019; Assink et al. 2019). Infrasound signals are generated by natural phenomena such as microbaroms, volcanoes and meteorites, as well as by human-activities such as explosions in mines or nuclear tests. The infrasound waves travel along waveguides in the atmosphere, which are formed by vertical variations in wind and temperature. Therefore, similar to seismic waves traveling through

the solid earth, the properties of the medium of propagation get encoded along the path of propagation and amplitude of the infrasound waves.

Through the tool of inverse theory, it is thus feasible to estimate the characteristics of the medium of propagation that explain a set of observations of infrasound data. Such is the effort that has been made by different groups working with infrasound observations around the world (see Assink et al. 2019, for a review). For example, Drob et al. (2010) proposed the parameterization of the adiabatic sound speed and wind profiles in 1D atmospheric models in terms of basis functions extracted from the singular value decomposition (SVD) of a population of historical profiles for the area of interest. In this way, the solution space was reduced to the estimation of scalar coefficients that multiplied by the basis functions produced the atmospheric profiles that explained the infrasound observations. Similar approaches were then followed by Lalande et al. (2012) and Assink et al. (2013).

Model simplification is generally required when working with infrasound observables to estimate atmospheric model updates. The reason is that the number of independent observations is normally much smaller than the number of model parameters to update, which makes the inverse problem strongly ill-posed. Alternatively, the size of the solution space can be reduced by imposing constraints (e.g., Vera Rodriguez et al. 2012; Vera Rodriguez & Kazemi 2016). In fact, the parameterization proposed by Drob et al. (2010) bounds the solution space to those models that are a linear combination of the chosen basis functions. This type of constraint preserves the most significant statistical properties of the atmosphere within the time span of the population of profiles used in the SVD, although it can be limiting or of little help in regions and/or time periods with dynamic atmospheric conditions.

Previous efforts to solve the inversion have resorted to parameterizations that follow the classical least-squares formalism, either based on Fréchet derivatives (Lalande et al. 2012) or with a Bayesian formulation (Assink et al. 2013). These attempts introduced additional model simplifications, such as fixing some of the profiles during the inversion (e.g., adiabatic sound speed), and/or inverting only for the upper atmospheric layers of the models.

In the current work, we consider a more general representation of the problem, in which the inversion is achieved via a solver of the heuristic type. The objective is to minimize a cost function, where the cost can be estimated either via least-squares or any other ad hoc metric. This offers flexibility not only to select convenient metrics to assess the merit of a solution, but also to easily incorporate different types of constraints without the need to reformulate the optimization, for example, by recalculating partial derivatives. In fact, the cost function does not need to be differentiable as required in classical methods using least-squares minimization.

To alleviate the ill-posedness of the problem, we bound the temperature and wind profile solution space to a region in the vicinity of the members of ERA5 ensemble reanalysis models (from now on ERA5-ensembles, Hersbach & Dee 2016; Hersbach et al. 2019). Then, we solve the optimization using a heuristic-learning algorithm previously developed to solve a similar inversion problem in passive seismics (Vera Rodriguez 2019). In this way, we not only estimate an updated model consistent with our infrasound observations, but also identify the members of the ERA5-ensemble that lie closer to it. The performance of the method is demonstrated using observations of infrasound waves produced by regular explosions at a site in Finland (Gibbons et al. 2015, 2019).

Recently, Vanderbecken et al. (2020) also looked at the problem of identifying members from ensemble models that were more likely representative of the atmospheric state based on their consistency with infrasound observations. The approach was applied to infrasound signals generated by the Mount Etna volcano. In this case, backazimuth and trace velocity observations were input to a Bayesian algorithm, which assigned a likelihood to each of the ensemble members. Different to the work presented here, the updates necessary to make any particular ensemble member consistent with the infrasound observations were not part of the estimations.

Also recently, Amezcua et al. (2020) performed an off-line data assimilation experiment where an Ensemble Kalman filter was applied to update the representation of cross-wind estimations into ERA5-ensembles. The cross-winds were estimated based on the measured travel-time and backazimuth deviation of infrasound arrivals from 598 explosions and an analytical formula (Blixt et al. 2019, see Section 2 in this article for further descriptions and references regarding this explosion dataset.). In this case, a single value of cross-wind was assimilated to update a particular model. This limits the constraint that is attainable with the infrasound information. Therefore, in this work we opt to use the three primary observables derived from the infrasound data (i.e., backazimuth, trace velocity and travel time).

In short, the contributions of this work can be summarized as: inverting for atmospheric wind and temperature profiles without restricting the solution space to atmospheric states that are linear combinations of previous states. Instead, we constrain the inversion by bounding the solution space with uncertainties that summarize the current atmospheric knowledge from direct and indirect measurements, and physical models. As a result of the inversion setting, our results can be directly related to the ensemble models used to bound the solution space, so that, the members of the ensemble that are more consistent with the infrasound observations can be identified.

We start the description in the following section by introducing the infrasound dataset and atmospheric models used to test the inversion. Thereafter, the parameterization of the problem is described together with the strategies followed to bound the solution space and achieve the optimization. Finally, we present detailed results of the inversion applied to an explosion from the real dataset, followed by our conclusions and future directions of work. Additional example results are also provided as complementary information.

2   THE HUKKAKERO EXPLOSION DATASET AND THE ATMOSPHERIC MODEL ENSEMBLES

The Hukkakero dataset consists of a series of explosions that happen regularly during August and September at the site of Hukkakero in Finland (67.94° N, 25.84° E) (Gibbons et al. 2007; Liszka & Kvaerna 2008). Both seismic and infrasound waves generated by the blasts are regularly detected at the array station ARCES (69.53° N, 25.51° E) located in northern Norway. Gibbons et al. (2015, 2019) described details of the dataset, including the processing conducted to extract the parameters arrival back azimuth (θ_{obs}) and trace velocity (v^{app}). Apart from θ_{obs} and v^{app}, total propagation time (T) is also an observation. Therefore, any one explosion provides with three points to fit during an inversion process (i.e., under the knowledge of the source position).

Blixt et al. (2019) estimated the uncertainty of the backazimuths extracted from this dataset to be in the range of 1.0° to 1.5°. Following a similar analysis for the apparent velocity yields uncertainties in the order of 10 m/s. Taking into account that these uncertainties are approximations obtained with an empirical analysis (see Blixt et al. 2019, Section 2C for details), we consider more conservative values of 0.5° and 5 m/s for the inversion process. For uncertainty in arrival time, we note that our array processing output is calculated over 10 s windows stepped with 1 s increments. Therefore, we consider reasonable to assume the uncertainty in arrival time estimation to be 1 s.

As noted in Blixt et al. (2019), ARCES is located within the classical shadow-zone distance from Hukkakero, suggesting that the arrivals detected at the station correspond to stratospheric reflections rather than refracted waves (e.g., Chunchuzov et al. 2015b,a). Using ray tracing for a fan of shooting elevation angles through ERA-interim atmospheric reanalysis models, Blixt et al. (2019) conducted a grid search to estimate the reflection-altitudes that minimized the difference between modeled and observed propagation times for 598 Hukkakero explosions. This exercise assumed that the atmospheric models represented reasonably well the infrasound propagation.

Since the objective of the inversion developed in the current work is to update the atmospheric models, the reflection altitude that explains an observed propagation time must also be updated in a self-consistent manner. This is achieved by including this altitude as part of the inverted model parameters.

The atmospheric models to update with the inversion are extracted from the ERA5 ensemble product. The ERA5-ensembles are the latest type of reanalysis models generated by the ECMWF. This product has global coverage and assimilates observations from satellites, land stations, buoys, radiosondes, aircrafts and ships. The ensemble models are available at 3-hour intervals with a 63 km horizontal resolution in 137 vertical levels from surface up to an altitude of 0.01 hPa, i.e., around 80 km (Hersbach & Dee 2016). The ERA5 product also includes single high-resolution realizations at temporal and horizontal resolutions of 1 hour and 31 km, respectively. In this work, however, we only use the ensembles so that we can derive uncertainties from the members. The ECMWF has made publicly available ERA5-ensembles from 1979 up to now with a delay of within 5 days from real time (Copernicus Climate Change Service (C3S) 2017).

In the context of infrasound studies using ensemble reanalysis models, Smets et al. (2015) studied probabilistic infrasound propagation by performing wave-propagation simulations using the ensemble members of the ECMWF Ensemble Data Assimilation (EDA) system analysis product. Averbuch et al. (2020) also applied the EDA ensemble model product in atmospheric infrasound propagation modelling when analyzing how to estimate depth and strength of submerged explosion sources from infrasound data.

3   PARAMETERIZATION OF THE PROBLEM

The cost function C to optimize is represented as

$$C = \mathcal{O}(\mathbf{m}, \mathbf{d}) , \tag{1}$$

where $\mathbf{m}$ and $\mathbf{d}$ are vectors that contain all the model parameters and observations, respectively, and $\mathcal{O}$ is an operator. The representation in 1 is general on purpose, as this gives flexibility to incorporate different types of variable manipulations and operations within $\mathcal{O}$. The operator $\mathcal{O}$ consists of:

(i) Using the model parameters to produce a forecast of the observations.

(ii) Evaluating the cost of the model parameters by comparing the forecast with the observations using a metric of choice.

The elements of vector $\mathbf{m}$ in our problem are the altitude of reflection of the infrasound arrival, and the profiles of temperature, zonal (W-E) and meridional (S-N) winds of an atmospheric model (vertical wind is neglected). The vector $\mathbf{d}$, on the other hand, contains the observations of θ_{obs}, v^{app} and T of a corresponding Hukkakero explosion. As the source and receiver positions are fixed, this information is hard-coded inside $\mathcal{O}$. Consequently, the first step in our operator $\mathcal{O}$ consists of using ray tracing with $\mathbf{m}$ to produce a forecast of the elements of $\mathbf{d}$.

We compute eigenray trajectories, in this case reflection from a specified altitude joining Hukkakero with ARCES, using GeoAc (Keys 1981; Blom & Waxler 2012). More specifically, we use the ray tracer GeoAc3D, which considers wave propagation in a cartesian frame where the medium is moving and without resorting to the effective sound speed approximation. Then, we use the geometry from the eigenrays together with the model parameters $\mathbf{m}$ to estimate the forecast of the observations (i.e., $\theta_{obs}^{(f)}$, $v^{app(f)}$ and $T^{(f)}$, where the superscript (f) refers to a forecast of the variable). Eigenrays are computed setting an error tolerance of $0.5°$ in azimuthal direction. This tolerance is within the uncertainty in the infrasound observations and results in rays landing within 0.6 km from the center of the ARCES array, which has an approximate radius of 1.5 km (Gibbons et al. 2015). Notice that the actual ray tracing operates over adiabatic sound speed rather than temperature. In this work, all the model perturbations are performed over the temperature profiles and then fed into GeoAc3D, which internally converts them into adiabatic sound speed.

For the second step, we use the following cost metric:

$$\lambda = K \frac{W_1 E(\theta) + W_2 \frac{|v^{app} - v^{app(f)}|}{v^{app}} + W_3 \frac{|T - T^{(f)}|}{T}}{W_1 + W_2 + W_3} \, , \tag{2}$$

where

$$E(\theta) = \frac{\sqrt{\left(\sin \theta_{obs} - \sin \theta_{obs}^{(f)} \right)^2 + \left(\cos \theta_{obs} - \cos \theta_{obs}^{(f)} \right)^2}}{2} \, . \tag{3}$$

Equation 2 is a weighted average, which facilitates a ranking-by-priority for the fitting of the observations during the inversion. For example, observations with larger uncertainties can have smaller weights. Similarly, observations that reflect lower sensitivity to changes in the model parameters can also have lower weights. In this work, we use the weights $W_1 = 1$, $W_2 = W_3 = 3$. The smaller weight on the backazimuth is used because we observed lower sensitivity in this variable with respect to changes in the model parameters. The same behavior was reported by Vanderbecken et al. (2020) in their Bayesian inversion. Traveltime and trace velocity, on the other hand, display a comparable level of sensitivity. We observed that if their

weights are not equal, the algorithm often converges to solutions that fit the variable with larger weight within its uncertainty but not the other one.

The purpose of the normalizations in the fractions in the numerator of equation 2 are to remove scale differences, homogenise units, and to help ensure bounds in the cost function in the approximate range of $[0, \sim1)$. Function $E(\theta)$ is defined taking the same requirements into consideration and also to avoid ambiguities when comparing angles. In particular, setting $[0, \sim1)$ bounds in the cost function is critical for the performance of the heuristic solver used for the optimization (Vera Rodriguez 2019).

As we discuss in the following section, the algorithm is initialized with average profiles obtained from the members of ERA5-ensemble models. The cost of these initial atmospheric models is already small. Therefore, we prefer absolute values over the more commonly used squared differences to increase the cost of the initial models. For the same objective, we introduce the hyperparameter K. Using a value of $K = 60$ we ensure an initial cost closer to 1 in every inversion run.

3.1   Constraining of the solution space

The inversion problem that we attempt to solve is strongly ill-posed. This is because the number of model parameters is much larger than the number of independent observations. Without access to additional observations, this limitation can be alleviated by either incorporating constraints (e.g., regularization) and/or by reducing the number of model parameters. For the first alternative, we use average profiles calculated with the members of ERA5-ensemble models as starting point. In addition, we bound the solution space to the region delimited by profiles that are a multiple of standard deviations obtained from the same ensembles. The standard deviations obtained in this way display variability with altitude, reflecting the better availability of information to constrain these models at lower altitudes. Similarly, the standard deviations for temperature are small compared to those of winds, reflecting also the more accessible measurements of this property in the atmosphere.

Reducing the number of standard deviations to set the limits of the solution space has the risk of excluding solutions that explain best the infrasound data. On the other hand, extending the dimensions of the solution space increases the number and diversity of atmospheric models that can explain the observations. We find a reasonable trade-off by testing different multiples of the standard deviations to set the size of the solution space. We consider that the size of the solution space is reasonable when after running the algorithm multiple times the final solutions resemble each other and all explain the observations within their uncertainties.

Even after delimiting the boundaries of the solution space, the number of model parameters is still much larger compared to the number of observations. Thus, in order to further improve the constraint in the inversion, we simplify the ERA5-ensemble models to 1D layered versions and assume time-invariance during the propagation of the infrasound waves. Previous work suggests that these assumptions are reasonable within the distance range between Hukkakero and ARCES (e.g., Lalande et al. 2012; Assink et al. 2013).

For the altitude of reflection we try two different initial values. First, we run three inversions using 39 km as initialization point. This is about the average reflection altitude estimated by Blixt et al. (2019) for the extended dataset of explosions. After that, we run another three inversions moving the initialization point to 38 km. The purpose of trying different initial altitudes is to verify that the final solution converges toward similar values independently of the initialization point. In both cases, the solution space is bound at ± 1 km from the initial reflection altitude.

4   INVERSION ALGORITHM

The optimization of equation 1 requires a non-linear solver. The algorithm selected here is a simplified version of the heuristic solver described in Vera Rodriguez (2019). This algorithm was designed to solve a similar problem in passive seismics, although in that case, the source locations were also an unknown and the observations to fit were waveforms (see also Vera Rodriguez 2018; Vera Rodriguez & Le Calvez 2018). With the simplifications, the solver approaches more the logic behind particle swarm optimization (PSO) (Shi & Eberhart 1998), albeit with modified updating rules and contingencies to breakout from local minima.

The search for the optimization point consists in guiding a group of particles (swarm) as they explore the solution space. The coordinates of each swarm particle at any iteration are given by tentative solutions that they explore. The next exploratory move of a swarm particle is influenced by two poles of attraction: one is the best solution ever explored by that particular swarm particle and the second is the best solution ever explored by any of the particles in the swarm. This intends to simulate the behavior of birds in their search for food sources, which is the original purpose of the PSO algorithm (Shi & Eberhart 1998). The evaluation of what is a better solution is quantified by the cost function. This means in our application that ray tracing must be conducted at every iteration for every particle of the swarm, which makes the solver computationally expensive. The updating rules used in Vera Rodriguez (2019) improve the rate of convergence by simulating more closely the process of iterative design (Nielsen 1993) rather than bird swarms. Additionally, we implement the solver in parallel using a

workstation with 24 cores and a swarm of 96 particles. This means that, in every iteration, every core only needs to do ray tracing four times. Given the tight constraints imposed over the solution space, this was considered sufficient to identify significant and consistent minima. Unconstrained inversions in contrast require larger swarms with their particles well-spread over the solution space.

An important advantage of the heuristic solver is its flexibility, as it can optimize objective functions that are not differentiable, and permits to easily incorporate various types of constraints. The main disadvantage, on the other hand, is its computational cost, since the algorithm consists of an explicit exploration of the solution space, where success depends on a careful management of trade-offs.

Apart from simplifying the solver to handle a smaller type-set of model parameters, two other modifications were introduced. The first of them is a smoothness constraint. This constraint is applied over the temperature and wind profiles. The smoothing filter is a 79-point moving average, which is applied to the signals in two directions taking care of boundary effects by padding at the ends with the end members of the profiles. Before smoothing, the profiles are resampled to a homogeneous rate computed as half of the smallest distance between layers. After smoothing, the profiles are interpolated back to the original altitude points. This constraint is applied to every new solution to be explored by the swarm. It helps in stabilizing the ray tracing and also reduces the solution space, thus, adding robustness to the inversion process.

The second modification refers to the rule to accept or reject a new update for the solutions to be explored by the swarm. In PSO and the solver proposed by Vera Rodriguez (2019), an update ($\Delta \mathbf{m}$) is rejected and modified if it is larger than pre-specified, to some extent empirical, values $\mathbf{v}^{max}$. In our modified version, $\mathbf{v}^{max}$ is given by the standard deviations extracted from the ERA5-ensemble and the altitude bound. The update is then rejected and modified if the updated solution ($\mathbf{m}_{k-1} + \Delta \mathbf{m}_k$, where k is the iteration number) after smoothing is outside the limits given by the initial model and $\mathbf{v}^{max}$ (i.e., $\mathbf{m}_0 \pm \mathbf{v}^{max}$). This is how we establish hard boundaries to the solution space.

For all the other hyperparameters required to run the solver, we use the values reported in Vera Rodriguez (2019). The solutions obtained with this inversion setup are temperature and wind profiles that honour the variability with altitude of the uncertainties in the ERA5-ensemble. The solutions, including reflection altitude, are also consistent with the infrasound observations and their uncertainties.
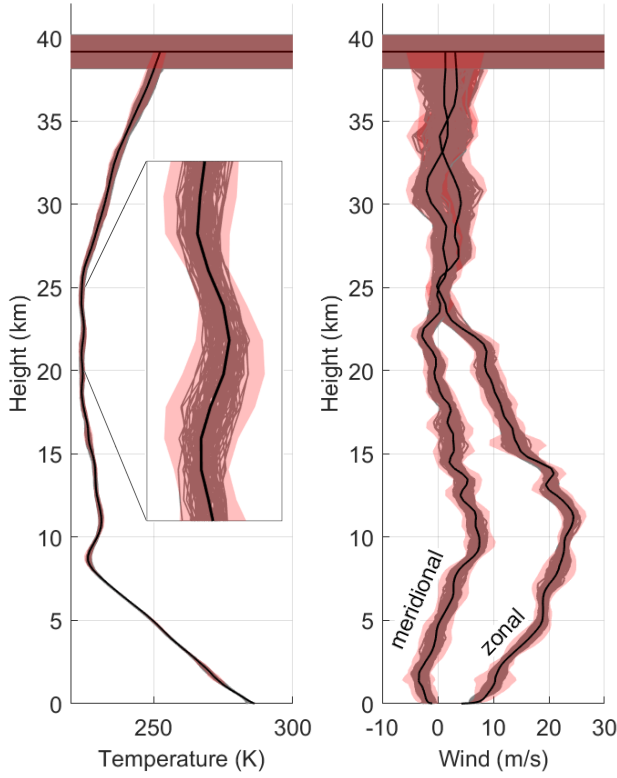
Figure 1. Example of inversion initialization. The initial model consists of temperature and wind profiles, and reflection altitude (black lines). The solution space is bounded with a multiple of the standard deviations of the initial model parameters (5σ in this example) and a limit manually specified in the case of the reflection altitude (red shaded areas). The search is conducted with a swarm of 96 particles whose initial position is determined by solutions (smoothed profiles) selected at random within the limits of the solution space (grey lines).

5 APPLICATION TO A HUKKAKERO EXPLOSION

We demonstrate the performance of the inversion using data from a blast on 24 August 2007 at around 11 am in Hukkakero. This example was selected at random within the catalogue of 598 explosions. Nevertheless, we observe that the inversion results are consistent with those from other explosions that we have also already analyzed (see complementary material). Figure 1 presents an example of initialization of the inversion for the selected example. The ERA5-ensemble for the time of the explosion is obtained via linear interpolation of the closest ensembles in time. The limits of the solution space for temperature and winds in this example are set as 5σ, where σ is a vector that contains the standard deviations extracted from the ERA5-ensemble. In the figure, it is visible how the uncertainty bounds increase with altitude and are also wider for winds than for temperature.

Figure 2 shows two examples of inversion results setting the limits of the solution space to

5σ. Each of the lines in the convergence plots (left panels in Figure 2) reflects the trajectory of a swarm particle as it finds better solutions during its exploration of the solution space. When the algorithm detects that the swarm is stuck in a local minimum (i.e., when all the convergence curves come together and do not decrease after a number of iterations) a perturbation is introduced to spread the swarm again (see Vera Rodriguez 2019, for details). This is expressed in the convergence curves as spikes. If the breakout from the local minimum is successful the swarm continues moving. After two failures, the algorithm gives up. Therefore, the end of the convergence curves is often preceded by at least two spikes. An exception is if the algorithm finds a solution with a lower cost than a pre-specified value without getting stuck, for example, as would be the case in a convex solution space. Given the tight constraints, the variations in ray trajectories between permissible models are allowed to be only significant enough as to explain the infrasound observations (Figure 3).

From testing the inversion with different limits of the solution space, we observed that using 5σ output models that reproduced the infrasound observations well within their uncertainty limits (Table 1). An illustration of the negative effects of increasing the bounds of the solution space is presented in Figure 4. In this Figure, inversion results setting the bounds to 10σ produced models that are more dissimilar between them and also with respect to the reference ensemble. On the other hand, convergence was achieved much quicker (often within 10 iterations) because of the larger number of solutions that could explain the observations. In contrast, reducing the bounds of the solution space increased the number of iterations because the number of solutions that explain the observations becomes limited (see Table 1). In our tests, 5σ provided a good trade-off to obtain solutions that resemble each other and produced forecasts within the uncertainty limits of the observations.

In these inversion results obtained with bounds at 5σ, the reflection altitude remained stable at around 38.5 km (see Table 1). Convergence toward this altitude was independent of whether the initialization point was above or below. For example, the results presented in Figure 2 correspond to initialization points at 39 km and 38 km, and to runs #1 and # 6, respectively, in Table 1. Both cases converged at or near this altitude of 38.5 km. Backazimuth and travel time were always better reproduced by the inverted models compared to trace velocity. This is likely related to the higher uncertainty in the estimations of trace velocity from the infrasound measurements in this dataset. Trace velocity in this example was underestimated by the ERA5-ensemble (see captions of Table 1). Thus, the updates introduced by the inversion produced ray trajectories with smaller inclination angles (see Figure 3). By favouring landing trajectories with smaller inclination angles rather than simply increasing temperature

Table 1. Inversion results for six runs of the algorithm using $5\boldsymbol{\sigma}$ to set the boundaries of the solution space. The infrasound observations are $\theta_{obs} = 175.7 \pm 0.5$ deg, $v^{app} = 337 \pm 5$ m/s and $T = 631 \pm 1$ s, and correspond to an explosion at Hukkakero from 24 August 2007 around 11 am. The forecast of the observations obtained with the average ensemble model (i.e., initial solution) is: $\theta_{obs}^{(0)} = 176.0$ deg, $v^{app(0)} = 329.1$ m/s and $T^{(0)} = 627.2$ s.

Run	Iterations	Cost	Altitude	$\theta_{obs}^{(f)}$	$\mathrm{d}\theta_{obs}$	$v^{app(f)}$	$\mathrm{d}v^{app}$	$T^{(f)}$	$\mathrm{d}T$
(#)	(#)	(%)	(km)	(deg)	(deg)	($\frac{\mathrm{m}}{\mathrm{s}}$)	($\frac{\mathrm{m}}{\mathrm{s}}$)	(s)	(s)
1	121	17	38.7	175.6	0.1	334.8	2.2	631.0	0.0
2	160	16	38.2	175.7	0.0	335.1	1.9	630.8	0.2
3	104	15	38.2	175.7	0.0	335.0	2.0	631.0	0.0
4	120	18	38.7	175.7	0.0	334.6	2.4	631.0	0.0
5	112	21	38.9	175.7	0.0	334.3	2.7	631.0	0.0
6	235	16	38.5	175.7	0.0	334.9	2.1	631.0	0.0

and winds at the bottom of the model, the updates maintained a trade off between increasing trace velocity without negatively affecting total travel time and honouring the smoothness constraint.

Looking at the cross differences between all the inverted profiles and all the ensemble members (Figure 5), the average modifications to the ERA5-ensemble necessary to explain the infrasound observations are more significant for the wind components than for temperature. This is understandable, given the larger uncertainty bounds specified for the winds. Also, as a result of the variation of uncertainty with altitude, it is visible that the average differences from the ERA5-ensemble are more significant above ∼30 km (see Figure 5d). Below this altitude the average deviations in inverted profiles from the ERA5-ensemble are within ±1.2 K and ±2.6 m/s, while above they lie within ±2.5 K and ±5.8 m/s. Another difference in the behavior of the average cross differences with respect to this altitude is their trend. In the case of temperature and zonal wind, below ∼30 km the deviations from the ERA5-ensemble oscillate around zero. Above this altitude the deviations define trends: positive deviations for zonal wind and negative deviations for temperature. The inversion results for meridional winds suggests a positive bias in the ERA5-ensemble with an average around 1.9 m/s along

most of the profiles (see Figure 5c and d). From $\sim$30 km, however, this bias shows continuous growth.

Despite that systematic comparisons between lidar soundings and ECMWF products have shown differences that are often larger than those displayed in our inversion results (Le Pichon et al. 2015; Hupe et al. 2019), the ERA5-ensemble models produced reasonable initial representations of infrasound propagation over different explosion-observations in this region of north Scandinavia (see complementary material for additional inversion examples). This good representation is partly expected because most of the region where infrasound propagates in this data set falls within the part of the models where measurements are normally available for assimilation. Thus, more significant corrections derived from the proposed inversion can be expected when analyzing returns from higher atmospheric altitudes.

6   CONCLUSIONS

We have presented an inversion scheme where complete 1D atmospheric models (i.e., temperature and wind components) can be updated with the use of infrasound observations from known sources. Furthermore, for the Hukkakero dataset that we used to demonstrate the performance of the inversion, the altitude of reflection of the infrasound waves was also an unknown that was part of the inverted model parameters.

The inverse problem is strongly ill-posed for which we had to simplify the atmospheric models to 1D, time-invariant versions. Furthermore, tight constraints were also necessary to reduce the dimensions of the solution space. We achieved this by bounding the solution space to the region around average atmospheric models obtained from ERA5-ensembles and by imposing smoothness in the solutions. Hence, the inverted/updated models explain the infrasound observations within their uncertainties and also lie in the vicinity of the ERA5-ensembles.

The inverted models displayed larger variations with respect to the reference ERA5-ensembles at stratospheric altitudes. This is consistent with a limited amount of direct measurements available to constrain the ERA5-ensembles in this region of the atmosphere. In this regard, the infrasound data becomes a valuable source of information to, at the least, point out which ensemble members should be preferred for further modelling tasks.

There are several lines to pursue in future work. For example, one possibility to modify the inversion is to weight the solutions explored by the swarm based on their proximity to a member of the ensemble. In this way, the distance between a solution and the ensemble could also be minimized. Another possibility is to incorporate additional physical constraints into

the model updates. This could be attained by explicitly honoring the relationship between wind and temperature within the algorithm.

In addition, a statistical assessment of the inversion method in the context of the corresponding model ensembles could be performed based on the full multi-year dataset of hundreds of Hukkakero explosions. Ideally, we would also prefer to confirm the inversion results using data from independent measurement technologies.

Moreover, extended data assimilation experiments might be initiated, building on the approaches developed by Amezcua et al. (2020): we could exploit that the current inversion provides altitude-dependent, both wind components – and not only cross-winds as were assimilated in Amezcua et al. (2020).

Such efforts are targeting as a long-term objective to let infrasound datasets contribute to numerical weather prediction models and an enhanced medium-range forecasting that takes further advantage of the predictive skills provided by a more reliable representation of stratospheric dynamics in models.

Finally, another line of future work consists of extending the data input to the inversion process by including travel-time, backazimuth, and apparent velocity estimates related to the full stratospheric arrival wavetrain, and not only a single data point associated with maximum array coherence. For higher-top models, we could also include mesospheric or lower thermospheric arrivals, hence both allowing layers at higher altitudes to be updated and also simultaneously improving the model constraints for lower altitudes.

REFERENCES

Amezcua, J., Näsholm, S., Blixt, E., & Charlton-Perez, A., 2020. Assimilation of atmospheric infrasound data to constrain tropospheric and stratospheric winds, *Quarterly Journal of the Royal Meteorological Society*, pp. 1–20.

Assink, J., Waxler, R., Frazier, W., & Lonzaga, J., 2013. The estimation of upper atmospheric wind model updates from infrasound data, *Journal of Geophysical Research*, **118**, 1–18.

Assink, J., Smets, P., Marcillo, O., Weemstra, C., Lalande, J., Waxler, R., & Evers, L., 2019. Advances in infrasonic remote sensing methods, Infrasound monitoring for atmospheric studies, pp. 605–632, eds Le Pichon, A., Blanc, E., & Huachecorne, A., Springer International Publishing, New York, 2nd edn.

Averbuch, G., Waxler, R., Smets, P., & Evers, L., 2020. Probabilistic inversion for submerged source depth and strength from infrasound observations, *The Journal of the Acoustical Society of America*, **147**(2), 1066–1077.

Blanc, E., Ceranna, L., Hauchecorne, A., Charlton-Perez, A., Marchetti, E., Evers, L., Kvaerna, T., Lastovicka, J., Eliasson, L., Crosby, N., Blanc-Benon, P., Le Pichon, A., Brachet, N., Pilger, C., Keckhut, P., Assink, J., Smets, P. M., Lee, C., Kero, J., Sindelarova, T., Kämpfer, N., Rüfenacht, R., Farges, T., Millet, C., Näsholm, S., Gibbons, S., Espy, P., Hibbins, R., Heinrich, P., Ripepe, M., Khaykin, S., Mze, N., & Chum, J., 2018. Toward an improved representation of middle atmospheric dynamics thanks to the ARISE project, *Surveys in Geophysics*, **39**(2), 171–225.

Blanc, E., Pol, K., Le Pichon, A., Hauchecorne, A., Keckhut, P., Baumgarten, G., Hildebrand, J., Höffner, J., Stober, G., Hibbins, R., Espy, P., Rapp, M., Kaifler, B., Ceranna, L., Hupe, P., Hagen, J., Rüfenacht, R., Kämpfer, N., & Smets, P., 2019. Middle atmosphere variability and model uncertainties as investigated in the framework of the arise project, in *Infrasound Monitoring for Atmospheric Studies*, pp. 845–887, Springer.

Blixt, E., Näsholm, P., Gibbons, S., Evers, L., Charlton-Perez, A., Orsolini, Y., & Kværna, T., 2019. Estimating tropospheric and stratospheric winds using infrasound from explosions, *The Journal of the Acoustical Society of America*, **146**, 973–982.

Blom, P. & Waxler, R., 2012. Impulse propagation in the nocturnal boundary layer: Analysis of the geometric component, *The Journal of the Acoustical Society of America*, **131**(5), 3680–3690.

Charlton-Perez, A., Baldwin, M., Birner, T., Black, R., Butler, A., Calvo, N., Davis, N., Gerber, E., Gillett, N., Hardiman, S., Kim, J., Krüger, K., Lee, Y., Manzini, E., McDaniel, B., Polvani, L.,

Reichler, T., Shaw, T., Sigmond, M., Son, S., Toohey, M., Wilcox, L., Yoden, S., Christiansen, B., Lott, F., Shindell, D., Yukimoto, S., & Watanabe, S., 2013. On the lack of stratospheric dynamical variability in low-top versions of the CMIP5 models, *Journal of Geophysical Research: Atmospheres*, **118**(6), 2494—-2505.

Chunchuzov, I. & Kulichkov, S., 2019. Internal gravity wave perturbations and their impacts on infrasound propagation in the atmosphere, Infrasound monitoring for atmospheric studies, pp. 551—-590, eds Le Pichon, A., Blanc, E., & Huachecorne, A., Springer International Publishing, New York, 2nd edn.

Chunchuzov, I., Kulichkov, S., Perepelkin, V., Popov, O., Firstov, P., Assink, J., & Marchetti, E., 2015a. Study of the wind velocity-layered structure in the stratosphere, mesosphere, and lower thermosphere by using infrasound probing of the atmosphere, *Journal of Geophysical Research: Atmospheres*, **120**(17), 8828–8840.

Chunchuzov, I., Kulichkov, S., Popov, O., Perepelkin, V., Vasil'ev, A., Glushkov, A., & Firstov, P., 2015b. Characteristics of a fine vertical wind-field structure in the stratosphere and lower thermosphere according to infrasonic signals in the zone of acoustic shadow, *Izvestiya, Atmospheric and Oceanic Physics*, **51**, 57–74.

Copernicus Climate Change Service (C3S), 2017. ERA5: Fifth generation of ECMWF atmospheric reanalyses of the global climate. Copernicus Climate Change Service Climate Data Store (CDS), March 2020.

Dahlman, O., Mykkeltveit, S., & Haak, H., 2009. *Nuclear test ban: converting political visions to reality*, Springer Science & Business Media.

Domeisen, D., Butler, A., Charlton-Perez, A., Ayarzagüena, B., Baldwin, M., Dunn-Sigouin, E., Furtado, J., Garfinkel, C., Hitchcock, P., Karpechko, A., Kim, H., Knight, J., Lang, A., Lim, E., Marshall, A., Roff, G., Schwartz, C., Simpson, I., Son, S., & Taguchi, M., 2020a. The role of the stratosphere in subseasonal to seasonal prediction: 1. predictability of the stratosphere, *Journal of Geophysical Research: Atmospheres*, **125**(2), 1–17.

Domeisen, D., Butler, A., Charlton-Perez, A., Ayarzagüena, B., Baldwin, M., Dunn-Sigouin, E., Furtado, J., Garfinkel, C., Hitchcock, P., Karpechko, A., Kim, H., Knight, J., Lang, A., Lim, E., Marshall, A., Roff, G., Schwartz, C., Simpson, I., Son, S., & Taguchi, M., 2020b. The role of the stratosphere in subseasonal to seasonal prediction: 2. predictability arising from stratosphere-troposphere coupling, *Journal of Geophysical Research: Atmospheres*, **125**(2), 1–20.

Drob, D., 2019. Meteorology, climatology, and upper atmospheric composition for infrasound propagation modeling, Infrasound monitoring for atmospheric studies, pp. 485—-508, eds Le Pichon, A., Blanc, E., & Huachecorne, A., Springer International Publishing, New York, 2nd edn.

Drob, D., Meier, R., Picone, J., & Garcés, M., 2010. Inversion of infrasound signals for passive atmospheric remote sensing, Infrasound monitoring for atmospheric studies, pp. 701–732, eds Le Pichon, A., Blanc, E., & Huachecorne, A., Springer International Publishing, New York, 1st edn.

Ehard, B., Malardel, S., Dörnbrack, A., Kaifler, B., Kaifler, N., & Wedi, N., 2017. Comparing ECMWF high-resolution analyses to lidar temperature measurements in the middle atmosphere, *Quarterly Journal of the Royal Meteorological Society*, **144**(712), 633—-640.

Gibbons, S., Ringdal, F., & Kværna, T., 2007. Joint seismic-infrasonic processing of recordings from a repeating source of atmospheric explosions, *The Journal of the Acoustical Society of America*, **122**(5), EL158–EL164.

Gibbons, S., Asming, V., Eliasson, L., Fedorov, A., Fyen, J., Kero, J., Kozlovskaya, E., Kværna, T., Liszka, L., Näsholm, P., Raita, T., Roth, M., Tiira, T., & Vinogradov, Y., 2015. The European Arctic: A Laboratory for Seismoacoustic Studies, *Seismological Research Letters*, **86**(3), 917–928.

Gibbons, S., Kværna, T., & Näsholm, S., 2019. Characterization of the infrasonic wavefield from repeating seismo-acoustic events, in *Infrasound Monitoring for Atmospheric Studies*, pp. 387–407, Springer.

Hersbach, H. & Dee, D., 2016. ERA5 reanalysis is in production, *ECMWF Newsletter*, **147**, 7.

Hersbach, H., Bell, B., Berrisford, P., Horányi, A., Muñoz Sabater, J., Nicolas, J., Radu, R., Schepers, D., Simmons, A., Soci, C., & Dee, D., 2019. Global reanalysis: goodbye ERA-Interim, hello ERA5, *ECMWF Newsletter*, **159**, 17–24.

Hersbach, H., Bell, B., Berrisford, P., Hirahara, S., Horanyi, A., Muñoz-Sabater, J., Nicolas, J., Peubey, C., Radu, R., Schepers, D., Simmons, A., Soci, C., Abdalla, S., Abellan, X., Balsamo, G., Bechtold, P., Biavati, G., Bidlot, J., Bonavita, M., De Chiara, G., Dahlgren, P., Dee, D., Diamantakis, M., Dragani, R., Flemming, J., Forbes, R., Fuentes, M., Geer, A., Haimberger, L., Healy, S., Hogan, R., Hólm, E., Janisková, M., Keeley, S., Laloyaux, P., Lopez, P., Lupu, C., Radnoti, G., de Rosnay, P., Rozum, I., Vamborg, F., Villaume, S., & Thépaut, J., 2020. The ERA5 global reanalysis, *Quarterly Journal of the Royal Meteorological Society*.

Hupe, P., Ceranna, L., Pilger, C., de Carlo, M., Le Pichon, A., Kaifler, B., & Rapp, M., 2019. Assessing middle atmosphere weather models using infrasound detections from microbaroms, *Geophysical Journal International*, **216**(3), 1761—-1767.

Kazutoshi, O., Junichi, T., Hiroshi, K., Masami, S., Shinya, K., Hiroaki, H., Takanori, M., Nobuo, Y., Hirotaka, K., T., K., Shinji, K., Koji, W., Koji, K., Ryo, O., Tomoaki, O., M., N., & Ryusuke, T., 2007. The JRA-25 reanalysis, *Journal of the Meteorological Society of Japan. Ser. II*, **85**(3), 369–432.

Keys, R., 1981. Cubic convolution interpolation for digital image processing, *IEEE Transactions on Speech and Signal Processing*, **29**(6), 1153–1160.

Khaykin, S. M., Hauchecorne, A., Wing, R., Keckhut, P., Godin-Beekmann, S., Porteneuve, J., Mariscal, J.-F., & Schmitt, J., 2020. Doppler lidar at Observatoire de Haute Provence for wind profiling up to 75 km altitude: performance evaluation and observations, *Atmospheric Measurement Techniques*, pp. 1–22, Accepted for publication.

Lalande, J.-M., Sebe, O., Landes, M., Blanc-Benon, P., Matoza, R., Le Pichon, A., & Blanc, E.,

2012. Infrasound data inversion for atmospheric sounding, *Geophysical Journal International*, **190**, 687–701.

Le Pichon, A., Assink, J., Heinrich, P., Blanc, E., Charlton-Perez, A., Lee, C., Keckhut, p., Hauchecorne, A., Rüfenacht, R., Kämpfer, N., Drob, D., Smets, P., Evers, L., Ceranna, L., Pilger, C., Ross, O., & Claud, C., 2015. Comparison of co-located independent ground-based middle atmospheric wind and temperature measurements with numerical weather prediction models, *Journal of Geophysical Research: Atmospheres*, **120**(16), 8318–8331.

Le Pichon, A., Blanc, E., & Hauchecorne, A., 2019. *Infrasound monitoring for atmospheric studies*, Springer International Publishing, New York, 2nd edn.

Lee, C., Smets, P., Charlton-Perez, A., Evers, L., Harrison, G., & Marlton, G., 2019. The potential impact of upper stratospheric measurements on sub-seasonal forecasts in the extra-tropics, Infrasound monitoring for atmospheric studies, pp. 889–910, eds Le Pichon, A., Blanc, E., & Huachecorne, A., Springer International Publishing, New York, 2nd edn.

Liszka, L. & Kvaerna, T., 2008. Propagation of infrasound from chemical explosions, *Inframatics Newsletter*, (20), 1–10.

Nielsen, J., 1993. Iterative user-interface design, *Computer*, **26**, 32–41.

Parker, W., 2016. Reanalyses and observations: What's the difference?, *Bulletin of the American Meteorological Society*, **97**(9), 1565–1572.

Podglajen, A., Hertzog, A., Plougonyen, R., & Zagar, N., 2014. Assessment of the accuracy of (re)analyses in the equatorial lower stratosphere, *Journal of Geophysical Research: Atmospheres*, **119**(11), 11166—-11188.

Shi, Y. & Eberhart, R., 1998. A modified particle swarm optimizer, in *Proceedings of the 1998 IEEE International Conference on Evolutionary Computation*, IEEE, IEEE, Anchorage, USA.

Simmons, A., Soci, C., Nicolas, J., Bell, B., Berrisford, P., Dragani, R., Flemming, J., Haimberger, L., Healy, S., Hersbach, H., Horanyi, A., Inness, A., Munoz-Sabater, J., Radu, R., & Schepers, D., 2020. Global stratospheric temperature bias and other stratospheric aspects of ERA5 and ERA5.1, Tech. rep., ECMWF Technical Memoranda.

Siskind, D. E. & Drob, D. P., 2014. *Use of NOGAPS-ALPHA as a Bottom Boundary for the NCAR/TIEGCM*, chap. 15, pp. 171–180, American Geophysical Union (AGU).

Smets, P., Evers, L., Näsholm, S., & Gibbons, S., 2015. Probabilistic infrasound propagation using realistic atmospheric perturbations, *Geophysical Research Letters*, **42**(15), 6510–6517.

Tan, D. G., Andersson, E., Kloe, J. D., Marseille, G.-J., Stoffelen, A., Poli, P., Denneulin, M.-L., Dabas, A., Huber, D., Reitebuch, O., Flamant, P., Le Rille, O., & Nett, H., 2008. The ADM-Aeolus wind retrieval algorithms, *Tellus A: Dynamic Meteorology and Oceanography*, **60**(2), 191–205.

Uppala, S., Kållberg, P., Simmons, A., Andrae, U., Da Costa Bechtold, V., Fiorino, M., Gibson, J., Haseler, J., Hernandez, A., Kelly, G., Li, X., Onogi, K., Saarinen, S., Sokka, N., Allan, R., Andersson, E., Arpe, K., Balmaseda, M., Beljaars, A., van de Berg, L., Bidlot, J., Bormann, N.,

Caires, S., Chevallier, F., Dethof, A., Dragosavac, M., Fisher, M., Fuentes, M., Hagemann, S., Hólm, E., Hoskins, B., Isaksen, L., Janssen, P., Jenne, R., Mcnally, A., Mahfouf, J., Morcrette, J., Rayner, N., Saunders, R., Simon, P., Sterl, A., Trenberth, K., Untch, A., Vasiljevic, D., Viterbo, P., & Woollen, J., 2005. The ERA-40 re-analysis, *Quarterly Journal of the Royal Meteorological Society*, **131**(612), 2961–3012.

Vanderbecken, P., Mahfouf, J., & Millet, C., 2020. Bayesian selection of atmospheric profiles from an ensemble data assimilation system using infrasonic observations of May 2016 Mount Etna eruptions, *Journal of Geophysical Research: Atmospheres*, **125**(2), e2019JD031168.

Vera Rodriguez, I., 2018. Full-waveform inversion of microseismic events to estimate origin times, locations, moment tensors and an attenuative velocity model, in *Conference Proceedings, 80th EAGE Conference and Exhibition*, EAGE, Copenhagen, Denmark.

Vera Rodriguez, I., 2019. A heuristic-learning optimizer for elastodynamic waveform inversion in passive seismics, *IEEE Transactions on Geoscience and Remote Sensing*, **57**, 2234–2248.

Vera Rodriguez, I. & Kazemi, N., 2016. Compressive sensing imaging of microseismic events constrained by the sign-bit, *Geophysics*, **81**(1), KS1–KS10.

Vera Rodriguez, I. & Le Calvez, J., 2018. Full-waveform inversion of microseismic events including moment tensors and layer depths, in *SEG Technical Program Expanded Abstracts*, SEG, Anaheim, California, USA.

Vera Rodriguez, I., Bonar, D., & Sacchi, M., 2012. Microseismic data denoising using a 3C group sparsity constrained time-frequency transform, *Geophysics*, **77**(2), V21–V29.
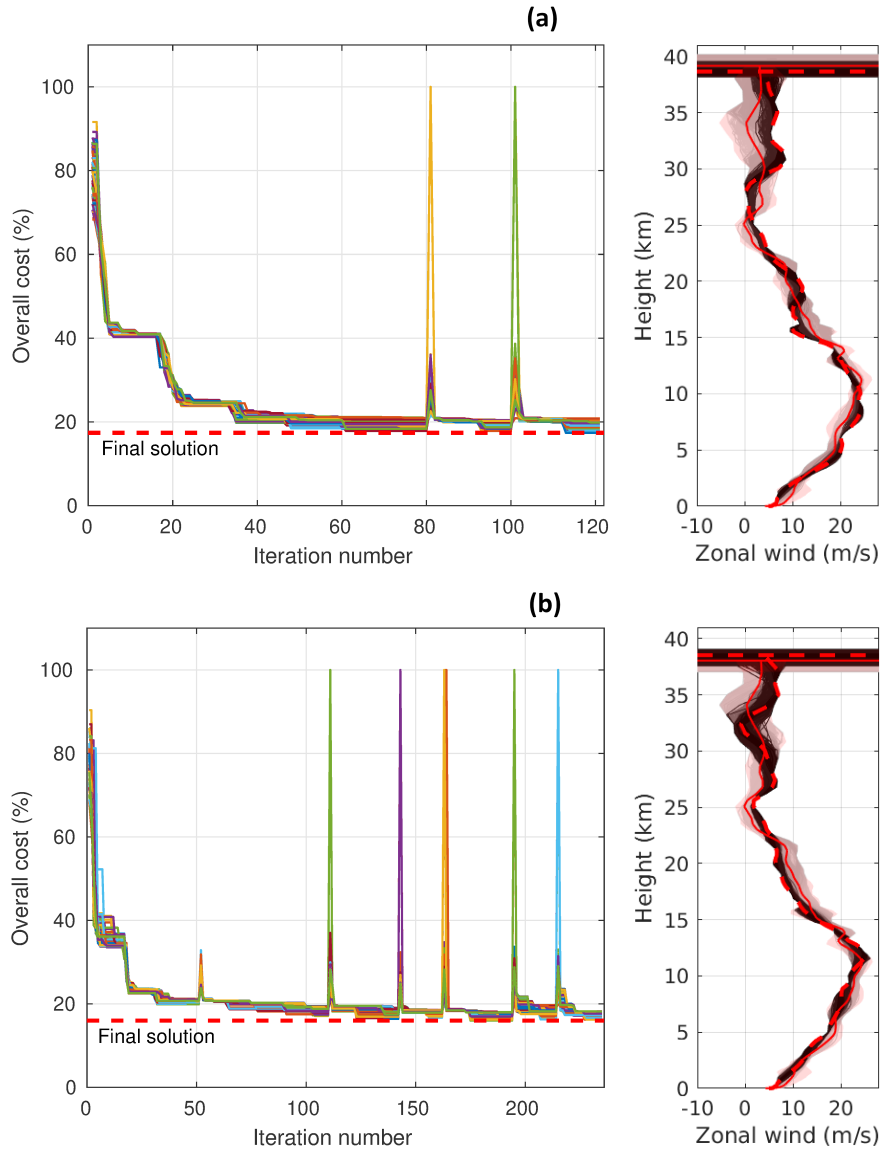
Figure 2. Examples of inversion results. Each line on the left panels tracks the convergence path of a swarm particle. The red dashed line marks the lowest misfit of any solution explored by the swarm. A spike along the convergence lines signals an attempt to breakout from a local minimum. The right panels are the corresponding zonal wind profiles and reflection altitudes at each of the iterations represented in the left panels. Lighter grey colors correspond to earlier iterations. The plots also show the initial solution (red solid lines), final solutions in each case (red dashed lines), and the bounds of the solution space (red shaded areas). These examples correspond to runs (a)#1 and (b)#6 in Table 1.
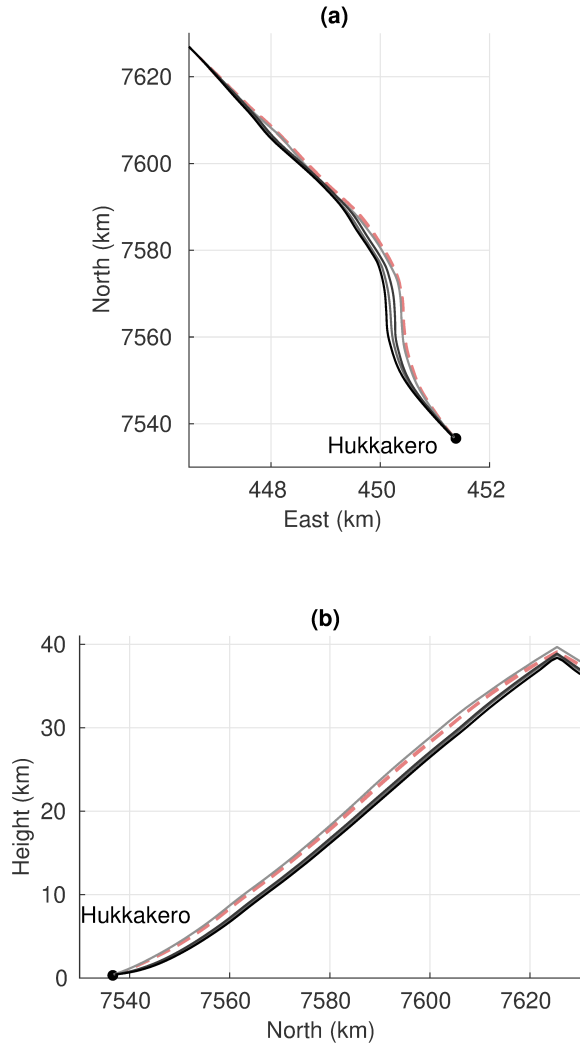
Figure 3. (a) Top and (b) side views of (half)ray trajectories traced during an inversion run. Red dashed lines are rays traced with the ten ERA-ensemble members. From lighter to darker colors, the solid lines are rays traced with models at iterations 1, 41, 81 and 121 during run #1 (see Table 1) for one swarm particle.
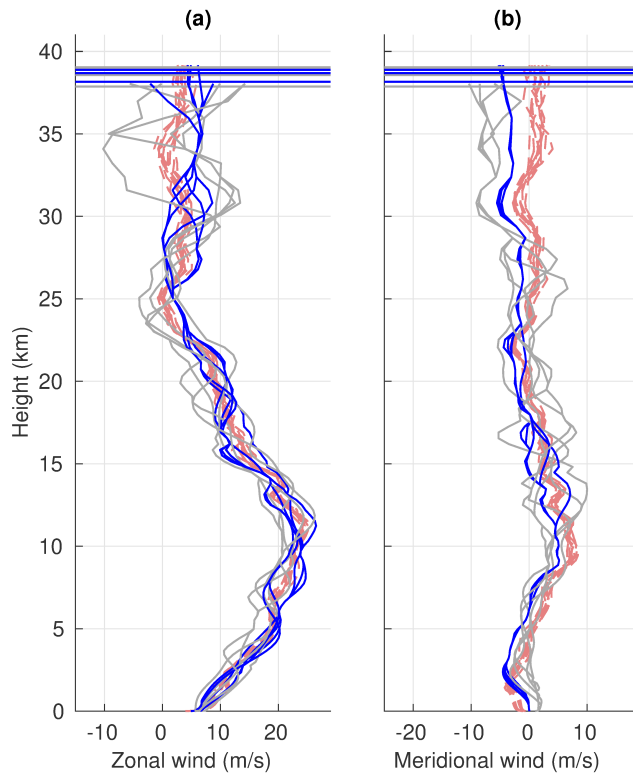
Figure 4. Comparison of ten inverted reflection altitudes together with (a) zonal and (b) meridional wind profiles obtained when setting the limits of the solution space to $5\boldsymbol{\sigma}$ (blue) and $10\boldsymbol{\sigma}$ (grey). Also plotted are the ten members of the ERA5-ensemble used to initialize the inversion in all cases (red).
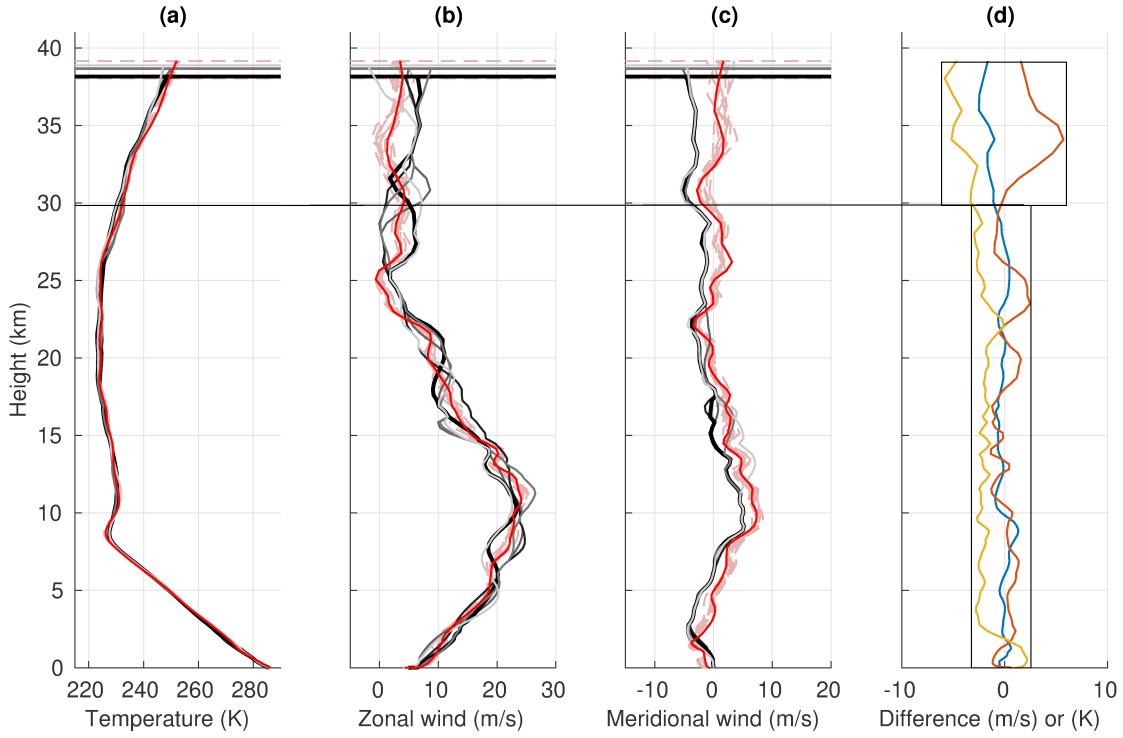
Figure 5. Inverted models for the inversion runs presented in Table 1. Lighter gray colors are models with larger cost. The model with the lowest cost has a thicker black line. Red dashed-lines are the members of the ERA5-ensemble used to initialize the inversion in all cases. Similarly, the horizontal, red dashed-lines represent the initial reflection altitudes (39 km and 38 km for inversion runs #1–#3 and #4–#6, respectively). The thicker, solid red line is the ensemble member that lies closest to the best inversion result. Panels (a), (b) and (c) display the model parameters. Panel (d) shows the average of the cross differences between all inversion results and all ensemble members for temperature (blue), zonal wind (orange) and meridional wind (yellow).